European Journal of Chemistry

One-pot method of synthesis and supercritical carbon dioxide drying of PVdF-HFP composite membranes

Agnieszka Martyla [1], Robert Przekop [2], Monika Osinska-Broniarz [1],
Mariusz Walkowiak [1] and Maciej Kopczyk [1]

[1] *Institute of Non-Ferrous Metals, Division in Poznan, Central Laboratory of Batteries and Cells, 12 Forteczna St., 61-362, Poznan, Poland*
[2] *Center of Advanced Technologies Adam Mickiewicz University, 89c Umultowska St., 61-614 Poznan, Poland*

** Corresponding author at: Institute of Non-Ferrous Metals, Division in Poznan, Central Laboratory of Batteries and Cells, 12 Forteczna St., 61-362, Poznan, Poland.
Tel.: +48.061.2797815. Fax: +48.061.2797897. E-mail address: agnieszka.martyla@claio.poznan.pl (A. Martyla).*

ARTICLE INFORMATION

KEYWORDS

ABSTRACT

This paper describes one-pot method of the synthesis and properties of composite polymer gel electrolytes based on poly(vinylidenefluoride-*co*-hexafluoropropylene) (PVdF-HFP). As the precursor of the inorganic filler tetraethyl orthosilicate (TEOS) and titanium *tetra-n-*butoxide ($Ti(OC_4H_9)_4$) were used. The drying of membranes with fillers was carried out with supercritical CO_2. The membranes and gel electrolytes have been examined structurally and electrochemically, showing favorable properties in terms of electrolyte uptake and electrochemical characteristics in Li-ion cells.

1. Introduction

Lithium ion cells are one of the fastest growing areas of energy storage technologies. This applies both to powering mobile devices and vehicles [1-3]. These cells are primarily based on liquid electrolytes [4]. New technologies involve use of gel-like electrolytes, which are supposed to ensure greater operational safety and minimizing the risk of spillage. The polymer matrix which is to act as the solid electrolyte must meet a number of requirements: have a good electrochemical stability related with redox processes at the lithium electrode, good compatibility with liquid electrolytes, low price, good mechanical strength and to be easy to manufacture and have good thermal resistance [5].

In recent years, poly(vinylidenefluoride-*co*-hexafluoro propylene) (PVdF-HFP) copolymer was widely tested as solid electrolyte in lithium ion batteries. It is well known fact that the addition of small particles of metal oxides (TiO_2, SiO_2) into the polymer matrix improves conductivity, thermal and mechanical stability and lithium cationic properties [6-9].

The subject of this work was the use of supercritical carbon dioxide as a drying agent for composite systems based on PVdF-HFP. In a further step composite polymer gel electrolyte for Li-ion batteries based on PVdF-HFP microporous polymer matrix and a family of SiO_2, TiO_2 and binary SiO_2-TiO_2 systems dried by this method were characterized. TiO_2, SiO_2 and SiO_2-TiO_2-PVdF-HFP systems were synthesized by a sol-gel method from TEOS and $Ti(OC_4H_9)_4$ precursors. The synthesis was carried out within the polymer matrix by condensation of reactants in a one-step method with the application of dibuthyl phthalate as porosity promoter. The drying of membranes with fillers was also carried out with supercritical CO_2. The structure of membranes was characterrized using XRD and SEM techniques, thermal analysis and FT-IR. Specific surface areas were determined by nitrogen absorption isotherms. Gel electrolytes, prepared by soaking of the dry composite membranes in lithium conducting liquid electrolyte, were subjected to a wide range of electrochemical tests.

2. Experimental

2.1. Instrumentation

Phase identification of samples was performed using an X-ray diffraction (XRD) powder diffractometer (Philips, PW

1050) using CuKα radiation and a Ni filter. The diffraction pattern were recorded in the range of 5 to 90 [2θ], with a step size of 0.04/[2θ] and 2s/step speed. The percent of crystallinity was determined from XRD data and it was calculated by dividing the total area of crystalline peaks by the total area under the diffraction curve (crystalline plus amorphous peaks) [10] using Automatic Powder Diffraction Philips software. The real area of the crystalline peaks and the amorphous peak can be determined from/by a computer software package performing a mathematical deconvolution of the peaks. The percentage of the crystalline polymer can be determined from Equation 1.

$$\% \text{ Crystallinity} = \frac{\text{Area under crystalline peaks}}{\text{Total area under all peaks}} x100 \qquad (1)$$

For the cross-section observation, the microporous membrane was freeze-fractured in liquid nitrogen and then sputter coated. Imaging the surface was performed with SEM electron microscopy (Phillips, 515 SEM).

Thermal stability of membranes was monitored by thermogravimetric analysis (TGA) and thermogravimetric analysis/differential thermal analysis (TGA/DTG) (Netzsch STA 409C 3F). TGA measurements were carried out under a nitrogen atmosphere at heating rate of 15 °C/min from 25 to 800 °C. The samples' weight was in the range of 5-10 mg. Nitrogen was used as a carrier gas with flow rate of 25 mL/min.

Surface studies were carried out using a Fourier Transform Infrared Spectroscopy/Attenuated Total Reflectance (FT-IR/ATR) with FT-IR spectrometer (Bruker, TENSOR 27) from ATR accessory (SPECAC). Measurement resolution was 4 cm^{-1}.

The porous structure was determined by low temperature (-196 °C) nitrogen adsorption measurements carried out on the Accelerated Surface Area and Porosimetry system model 2010 made by Micromeritics, using 200-300 mg of sample with the grain size fractions between 0.1 and 0.2 mm. Prior to nitrogen adsorption, all samples were outgassed at 623 K, at 0.4 Pa until a constant mass was reached. Both adsorptive and desorptive branch of the isotherm was taken in the range of p/p_0 0-1.

For the study of liquid phase uptake, small pieces were cut off from dry membranes. Once carefully dried and weighted, they were immersed in a container with pure propylene carbonate (anhydrous, 99.7%, Aldrich). At predefined moments in time, the membrane pieces were removed from the container, blotted lightly from the excess of liquid, weighted and immediately placed again in the container. Liquid phase uptake was followed as a result of swelling membrane weight increase:

$$\text{Membrane weight increase} = (m_t - m_0)/m_0 \times 100 \, [\%] \qquad (2)$$

where m_0 is the weight of dry membrane, m_t is the weight of membrane after a given time of swelling.

The ionic conductivity of composite gel polymer electrolytes is calculated from:

$$\sigma = L/(R_b \times A) \qquad (3)$$

where L and A represent thickness and area of the electrolyte specimen, respectively. R_b is the bulk resistance of the gel electrolyte obtained from complex impedance measurements.

For the conductivity measurements gel electrolytes were prepared by immersing round pieces of dry composite membranes (10 mm diameter) for 1 hour in a liquid electrolyte typical for Li-ion batteries, consisting of 1 M solution of LiPF$_6$ (Aldrich 99.99%) in 1:1 (*w:w*) mixture of ethylene carbonate (EC, anhydrous, Sigma-Aldrich 99%) and dimethyl carbonate (anhydrous, Sigma-Aldrich 99%). In the next step, the round pieces of membranes swelled in the liquid

electrolyte were placed in a two-electrode Swagelok-type cell with stainless steel electrodes. All these operations were conducted in a glove box, in dry argon atmosphere. The conductivities were determined at several temperatures (10-60 °C) on the basis of impedance spectra obtained by means of PARSTAT 2263 (Princeton Applied Research) impedance analyzer in the frequency range of 100 kHz - 1 Hz with 10 mV AC amplitude. Typically, each measurement was repeated several times to ensure good reproducibility of results. The cells were thermostated during measurements in a climatic chamber (Vötsch).

Activation energy for composite polymer gel electrolytes have been calculated from the equation:

$$\sigma = \sigma_0 \exp(-E_a/kT) \qquad (4)$$

where σ_0 is the pre-exponential factor, E_a is the activation energy, T is the absolute temperature in Kelvin scale and k is the Boltzmann constant.

2.2. Synthesis

The poly(vinylidenefluoride-*co*-hexafluoropropylene) was purchased from Kynar Flex, Atofina. The dibutyl phthalate from Merck, tetraethyl orthosilicate, tetrabutyl titanate and acetic acid were from Alfa Aesar.

The PVdF-HFP gels were prepared according to a method similar to the so-called Bellcore. PVdF-HFP copolymer was added to acetone together with dibutyl phthalate and precursor of inorganic fillers. Inorganic filler was created in *one step method* with the formation of the membrane by the simultaneous hydrolysis and condensation of the corresponding alkoxide precursor [11].

$$CH_3COOH + Si(OEt)_4 \rightarrow Si(OEt)_3(CH_3COO) + EtOH \qquad (5)$$

$$EtOH + CH_3COOH \rightarrow CH_3COOEt + H_2O \qquad (6)$$

$$H_2O + Si(OEt)_3(CH_3COO) \rightarrow HOSi(OEt)_3 + CH_3COOH \qquad (7)$$

$$2 \, HOSi(OEt)_3 \rightarrow (EtO)_3Si\text{-}O\text{-}Si(OEt)_3 + H_2O \qquad (8)$$

$$CH_3COOH + Ti(OEt)_4 \rightarrow Ti(Ot\text{-}Bu)_3(CH_3COO) + t\text{-}BuOH \qquad (9)$$

$$t\text{-}BuOH + CH_3COOH \rightarrow CH_3COOt\text{-}Bu + H_2O \qquad (10)$$

$$H_2O + Ti(Ot\text{-}Bu)_3(CH_3COO) \rightarrow HOTi(Ot\text{-}Bu)_3 + CH_3COOH \qquad (11)$$

$$2 \, HOTi(Ot\text{-}Bu)_3 \rightarrow (t\text{-}BuO)_3Ti\text{-}O\text{-}Ti(Ot\text{-}Bu)_3 + H_2O \qquad (12)$$
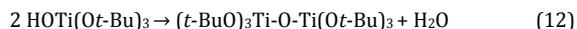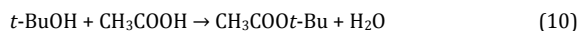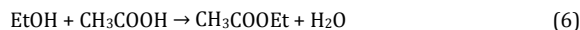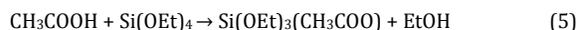
Such a synthesis strategy results from the experiments described in the work for the preparation of the gel systems of the oxides and hydroxides by hydrolysis and condensation in anhydrous solvents [12,13].

Tetraethyl orthosilicate (TEOS) was used as a source of silica. Tetrabutyl titanate (Ti(OC$_4$H$_9$)$_4$) was a titanium oxide source. The weight ratio of the filler precursor (as final oxide) to the copolymer was 1:10. Acetic acid (CH$_3$COOH) was added to methanol (CH$_3$OH) as a hydrolysis and condensation agent. Mixtures were stirred and heated at 45 °C for several hours. Each solution was cast on a glass plate, covered with a Petri dish and left for slow evaporation (5 days). The resulting membranes were immersed in an apparatus for drying under supercritical conditions of CO$_2$. The system was maintained at constant pressure of 1250psi and temperature of 35 °C for 6h. Next, the system was slowly depressurized for about 2 h at the same temperature. As soon as the depressurization process was completed, the resulting membranes were collected and kept in a desiccator for further use. The resulting samples were named respectively: PVdF-HFP, PVdF-HFP-SiO$_2$, PVdF-HFP-TiO$_2$, PVdF-HFP-SiO$_2$-TiO$_2$.
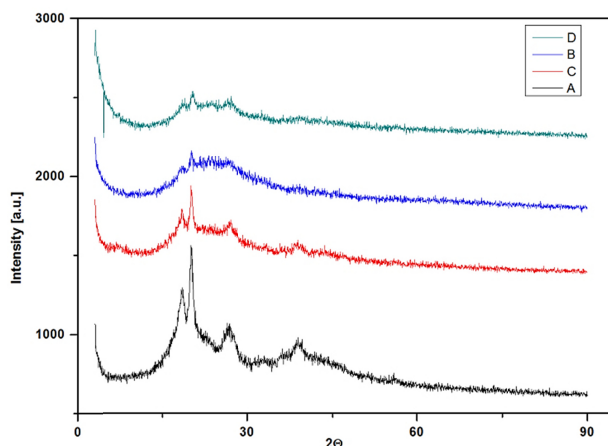
Figure 1. XRD pattern of A) PVdF-HFP, B) PVdF-HFP-SiO$_2$, C) PVdF-HFP-TiO$_2$, D) PVdF-HFP-SiO$_2$-TiO$_2$.
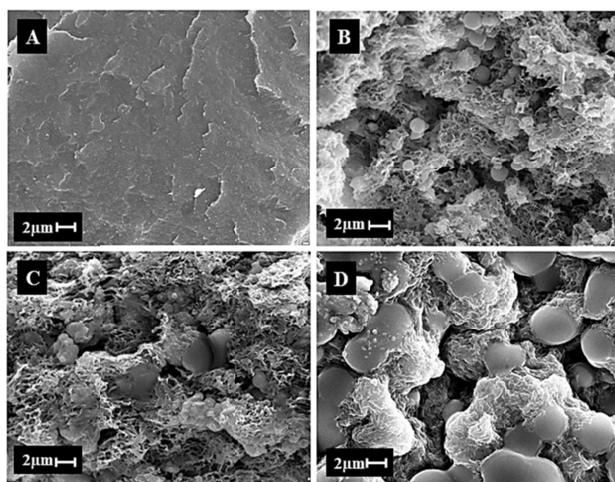

Figure 2. SEM image of composite membranes: A) PVdF-HFP, B) PVdF-HFP-SiO$_2$, C) PVdF-HFP-TiO$_2$, D) PVdF-HFP-SiO$_2$-TiO$_2$.

3. Results and discussion

It is well known that PVDF can crystallize mainly into three structures: α, β, and γ type [14], depending on the crystallization conditions. α type crystal structures were observed recently (Figure 1A). Peaks of interest here are at [2θ] 18.4, 20.0, 26.5 and 38.9 ° corresponding to 100, 020, 110, and 021 planes of crystalline PVdF. Diffractograms of the modified membranes are shown on Figures 1B-1D. The inorganic component mixed with the crystalline polymer led to the phase changes in the hybrid matrix, which was confirmed by the appearance of a non-crystalline phase. The additive of the SiO$_2$ increases the loss of intensity of the peak at 38.9 °, as in the case of binary oxide component addition. The smallest changes were observed for TiO$_2$-doped membranes, which caused only a decrease in intensity of reflections.

The intensities of the crystalline peaks further decreased, indicating the more amorphous type morphology of the composite membranes. We observe also the change of crystallinity of the composite. The calculated crystallinity of PVdF-HFP membranes was approximately 28%, while the crystallinity of PVdF-HFP membranes formed using TiO$_2$, SiO$_2$, SiO$_2$-TiO$_2$ as additives was 26, 5 and 5%, respectively. The crystallinity of doped membranes is lower than pure PVdF-HFP. The results can confirm the formation of particles of inorganic filler and its uniform distribution in the membrane [15].

The decrease of the crystallinity degree of the material is related to the formation of filler particles of a very small size and thus increase the role of the polymer chains interaction. A further consequence of these phenomena should be an increase the ionic conductivity of the material [16,17].

SEM observation was performed on the cross-sections of the membranes formed in liquid nitrogen. Figure 2 shows morphology of pure polymer (Figure 2A) and modified CO$_2$-dried composites membranes.

Results show that the addition of an inorganic filler has changed the structure, morphology and size of PVdF–HFP membrane pores. The nature of the structure of the PVdF-HFP is clearly observed in Figure 2A. In situ generated SiO$_2$ formed spherical particles build in the polymer network (Figure 2B). During synthesis, other fillers also are incorporated into the polymer network, causing a increase in porosity (Figure 2C, 2D).

This is confirmed by the surface area study (Table 1). Addition of the inorganic filler led to a large increase in BET surface area in comparison to non-modified PVdF-HFP. This is also reflected in the pore sizes.
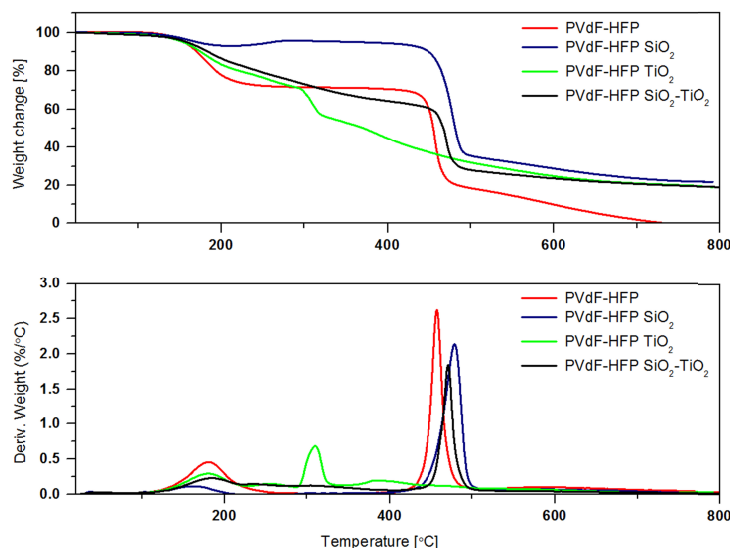
Figure 3. TG/DTG analysis of pure and modified membranes.

Biggest impact is observed for SiO_2, in case of which the membrane has six times larger specific surface area and the smallest pores in comparison to the unmodified PVdF-HFP.

Table 1. Comparison of surface area of membranes.

Sample	BET [m²/g]	Average pore diameter [nm]	Pore volume [cm³/g]
PVdF-HFP	6.14	3.44	0.07
PVdF-HFP-SiO₂	38.95	4.62	0.04
PVdF-HFP-TiO₂	15.65	4.77	0.02
PVdF-HFP-SiO₂-TiO₂	11.75	6.45	0.01

The TG measurements were performed to characterize the thermal stabilities of the composites. TG/DTG (at nitrogen atmosphere) curve of the membrane is shown in Figure 3. The curve shape shows preliminary mass loss in the temperature range of 170-190 °C. The mass loss of about 4% can be attributed to the removal of moisture or water and solvent absorbed by the sample during loading [18]. The mass loss is in agreement/compatible with the peak observed in the DTG curve at 171 °C for membrane with SiO_2 and at 186.6 °C for the rest of the samples.

It is observed at the thermogram that for the sample with TiO_2 the decomposition starts at 257 °C and also occurs at 308 °C. DTG curve of the sample shows peaks at 265 and 308 °C. This is well correlated with the mass loss of the sample observed in TG curve and is related to the degradation of the polymer side chains. The remaining 17 wt.% of the analyzed sample can be due to the presence of TiO_2 or due to the presence of CF-based PVdF-HFP polymer matrix. It is also observed that the complete decomposition of the sample takes place at 386 °C with the corresponding weight loss. The surface of TiO_2 nanoparticles is in fact modified by the alcohol molecules. The sharp exothermic peak at *ca.* 300 °C belongs to the decomposition of chemical absorption of organic species [18]. Addition of SiO_2 and SiO_2-TiO_2 binary system leads to a thermogram which indicates two weight losses correlated with peaks on DTG curves. It is also observed that the complete decomposition of the samples takes place between 450-500 °C. There is no appreciable weight loss above 520 °C. PVdF-HFP has a decomposition temperature of 457 °C. It was noted from the above analysis that addition of fillers to the polymer matrix slightly influences thermal stability of the electrolyte medium. Only the addition of SiO_2 increases thermal stability of PVdF-HFP. This sample starts to

decompose at 420 °C and the weight loss of about 50% is mainly due to the degradation of side chains of the polymer. This is confirmed by the peak observed in the DTG curve at around 480 °C.

The remaining 20 wt. % of the modified samples can be due to the presence of oxides or due to the presence of CF-based PVdF-HFP polymer matrix [18].

For pure PVdF-HFP spectra in Figure 4A vibrational bands at 760, 870 and 973 cm^{-1} can be assigned to crystals of PVdF-HFP phase [19]. Bands at 1060 and 1180 cm^{-1} are attributed to stretching vibrations of CF_2 and CF of the vinyl group respectively. The amorphous phase of PVdF-HFP is observed at 871 cm^{-1} [19]. Bands detected at 1148, 1203, 1179 and 1382 cm^{-1} are related to symmetrical and asymmetrical stretching vibrations of the CF_2 group. There was no phenomena in which any band disappeared when the fillers were added.

In the Figure 4B we observe a peak at 1100 cm^{-1}, which is assigned to Si-O-Si stretching vibration. Addition of TiO_2 reduces its intensity. A membrane with SiO_2-TiO_2 (Figure 4D) filler showed peaks at 1658 and 1572 cm^{-1} attributed to the bending vibration of -OH groups [20].

For all drying samples, the FT-IR spectra have almost the same shape as a pure PVdF-HFP which confirms the interacttion between inorganic fillers and oxygen atoms in the polymer leading to the formation of polymer complex [21].

Using the synthesis methods of TiO_2 from alkoxide precursors, the termination of the alkoxide groups may occur, which leads to the reduction of the contact among anatase grains [20]. This phenomenon leads to the reduction of interactions of grains and thus decreases the degree of their aggregation. This effect is visible in the absorption bands at 1464 and 1040-1130 cm^{-1} (Figure 4C), corresponding to C–H stretching and C–O vibration, respectively [22]. These characters were observed for alkoxy groups in many alkoxide-derived particles [23]. Broad band observed at about 3500 cm^{-1} is derived from the OH group stretching and results from the presence of water in the investigated samples. The presence of water confirms the occurrence of the hydrolysis and condensation processes of alkoxide precursors, described by the following reactions (Equation 3-10). Analysis of non-modified PVdF-HFP did not reveal presence of this band (Figure 4A).

Figure 5 illustrates how the membrane weights increase upon immersion in propylene carbonate. The solvent uptake after 1 hour of swelling is also presented in Figure 6.
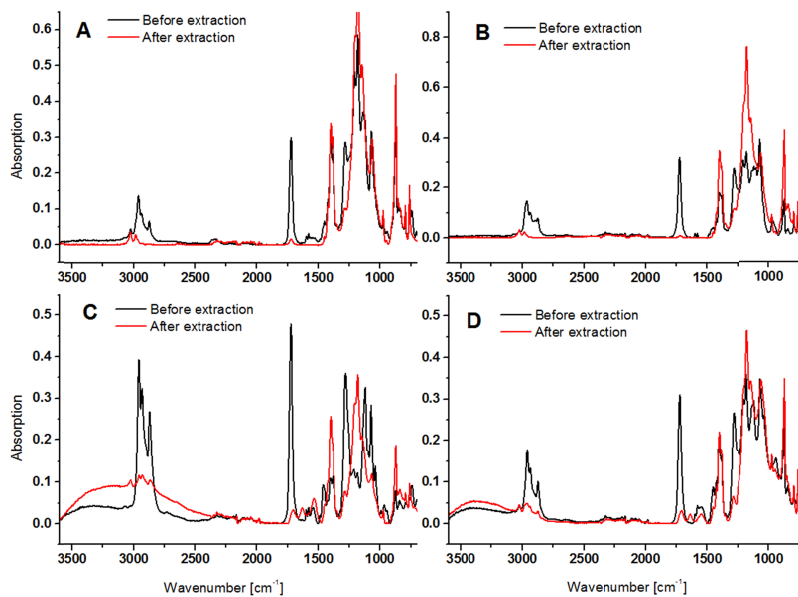
Figure 4. FT-IR spectra of pure and modified membranes: A) PVdF-HFP, B) PVdF-HFP-SiO₂, C) PVdF-HFP-TiO₂, D) PVdF-HFP SiO₂-TiO₂.
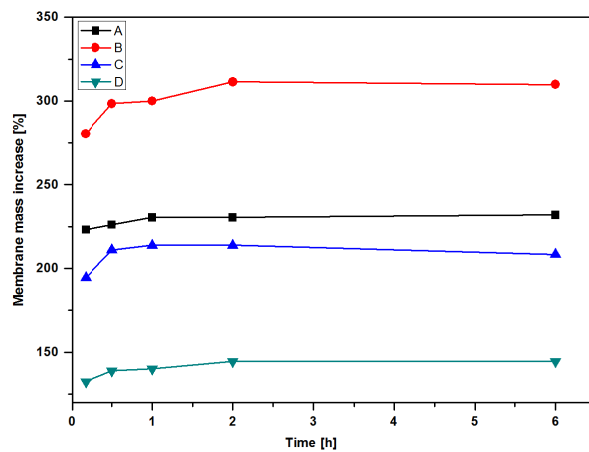
Figure 5. PC uptake of the composite polymer membrane as a function of time. PVdF-HFP, B) PVdF-HFP-SiO₂, C) PVdF-HFP-TiO₂, D) PVdF-HFP-SiO₂-TiO₂.
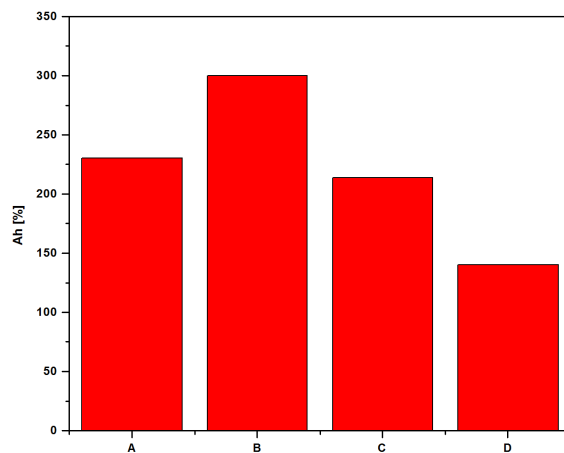
**Figure 6**. Value of absorption solution after 1 hour of swelling in PC. PVdF-HFP, B) PVdF-HFP-SiO₂, C) PVdF-HFP-TiO₂, D) PVdF-HFP-SiO₂-TiO₂.
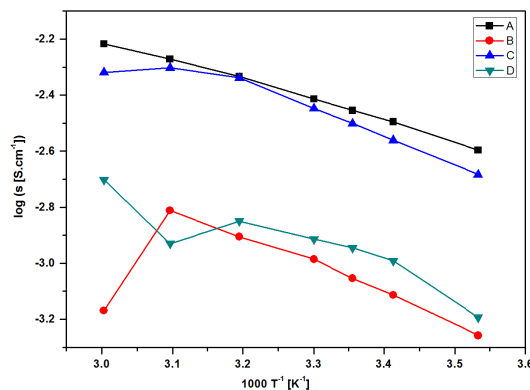
Figure 7. Temperature dependencies of ionic conductivities determined for the composite membranes presented as Arhenius plots: PVdF-HFP, B) PVdF-HFP-SiO₂, C) PVdF-HFP-TiO₂, D) PVdF-HFP-SiO₂-TiO₂.
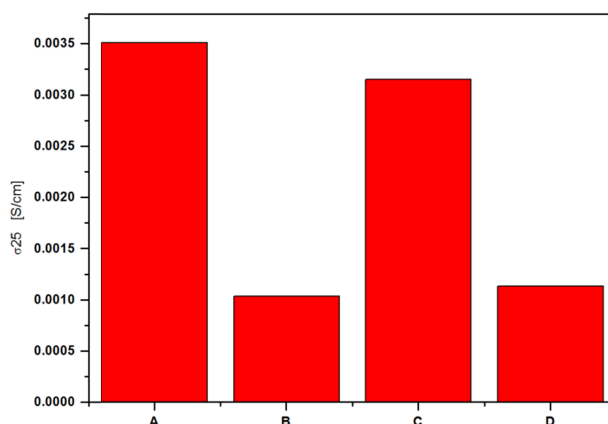

Figure 8. Specific conductivities of membranes at 25 °C: A) PVdF-HFP-SiO₂, B) PVdF-HFP-SiO₂-TiO₂, C) PVdF-HFP-TiO₂, D) PVdF-HFP.

Membranes with SiO_2 absorb solvent extremely well and much better than the membrane with no filler or with any other ceramic filler that was used in experimental work.

For all composite polymer membranes the maximum uptake is achieved quickly (about one hour). The observed solvent uptake after one hour of swelling is from about 140% for the hybrid filler up to 300% for the membrane with SiO_2. These values are comparable with literature data [24]. Membranes with hybrid SiO_2/TiO_2 fillers absorb solvent much less than all other test samples [25].

It is known that addition of inorganic fillers to the polymer electrolyte such as silica (SiO_2), alumina (Al_2O_3), titania (TiO_2, rutile or anatase), magnesium oxide (MgO) results in the improvement of ionic conductivity and mechanical and electrochemical parameters as well [26-28].

Figure 7 shows the temperature dependencies of ionic conductivity plot of PVdF-HFP based membranes. The ionic conductivity of composite gel polymer electrolytes is calculated from Equation 11.

The increase in conductivity with temperature can be linked to the decrease in viscosity and, hence, increases the chain flexibility of the electrolyte. As the temperature increases, the mobility and the dissociation rate of Li ions also increase, thus improving the conductivity of the electrolyte.

As temperature increases, the polymer expands and produces empty areas that cause species such as polymer segments, mobile ions or solvated molecules to move into these free volumes. The segmental movement of polymer promotes the transfer of ionic motion by allowing the ions to transfer from one site to another in the same polymer chain or

to neighboring polymer chain resulting in the increment of ionic conductivity [19].

As commonly found in composite materials, the conductivity is not a linear function of the filler concentration. The highest conductivity is for SiO_2 and TiO_2 filler. The binary system has almost the same conductivity as pure PVdF-HFP. This is associated with structure of membranes, when particles of oxide fillers are uniformly dispersed in the polymer matrix and can interact with other electrolyte components. This leads to the fast ion transport and consequently to the conductivity enhancement. The addition of SiO_2 to PVdF-HFP based gel polymer electrolyte increases the ionic conductivity [27] when thin layers of electrolyte adsorbed on the filler grain surfaces can ensure sufficiently favorable transport environment for ions.

The role of TiO_2 nanoparticles in the gel polymer electrolyte is well known. Addition of TiO_2 nanoparticles to PVdF-HFP polymer matrix leads to improvement of the ionic conductivity. Ion migration within nanopores may be promoted by higher TiO_2 dielectric constant, which is originated from its inherent dipole property. Relating to this role of TiO_2, it is well agreed that the nanoparticles can diminish the ion-aggregation in the electrolyte medium, which can be originated from their dielectric nature and/or chemical interaction between TiO_2 and PVdF-HFP [29,30].

In case of the membrane containing SiO_2-TiO_2 filler low crystallinity and low surface area lead to low conductivity [21]. In Figure 8 logarithms of specific conductivities at 25 °C have been plotted as a function of filler content. The specific conductivities at 25 °C range from 1.0×10^{-3} S/cm to 3.5×10^{-3}

S/cm. The highest conductivity was obtained for SiO_2, TiO_2, a binary filler, lead to lower conductivity than pure PVdF-HFP. It is the further evidence of the effect of the membrane structure on its conductivity and this is consistent confirmed by other observations [29,30].

Apparent activation energies have been calculated as a function of filler using the Equation 12. Activation energies and room temperature ionic conductivities of different compositions are summarized in Table 2. The minimum value of E_a is 0.141eV for the pure PVdF-HFP. There is an increase in E_a for a binary filler content. For the rest of samples the values of E_a indicate no clear correlation with the filler content.

Table 2. The value of activation energy as a function of filler.

Composite polymer gel electrolyte	E_a [eV]
PVdF-HFP	0.141
PVdF-HFP- SiO_2	0.142
PVdF-HFP-TiO_2	0.145
PVdF-HFP-SiO_2-TiO_2	0.175

4. Conclusions

1. Composite polymer-ceramic membranes were manu-factured by a modified Bellcore procedure, in which dibuthyl phthalate extraction and in-situ oxide formation were carried out simultaneously by the application of supercritical CO_2.
2. XRD patterns reveal that crystallinity degree of the polymer matrices decreased in the presence of fillers.
3. Gel electrolytes obtained by activation of dry membranes exhibit significant, very high conductivities, exceeding 6.06×10^{-3} Scm^{-1}.
4. The obtained results are promising from the point of view of possible application in Li-ion battery technologies.

PVdF-HFP-SiO_2, -TiO_2 and -SiO_2-TiO_2 composite polymer electrolyte membranes were studied to investigate the role CPD and inorganic filler on gel polymer electrolyte. The addition of filler to PVdF-HFP based gel polymer electrolyte allowed to obtain microporous composite polymer electrolyte. Reduction in crystallinity after addition of inorganic fillers and their interaction with the polymer were established from the XRD and FTIR studies. Incorporation of fine, well dispersed oxide particles prevents reorganization of polymer chains, resulting in a decrease in polymer crystallinity which gives rise to an increase in ionic conductivity and stabile thermal properties [30]. Morphological study shows porous structure of the membranes after supercritical CO_2 drying that can be more effective change of the structure and ionic conductivity. Based on these results it can be suggested that silica obtained by one-pot reaction method can be good filler for polymer electrolyte membranes.

Acknowledgements

References

[1]. Armand, M.; Tarascon, J. M. *Nature* **2008**, *451*, 652-657.
[2]. Dunn, B.; Kamath, H.; Tarascon, J. M. *Science* **2011**, *334*, 928-935.
[3]. Park, O. K.; Cho, Y.; Lee, S.; Yoo, H. C.; Song, H. K.; Cho, J. *Energy Env. Sci.* **2011**, *4*, 1621-1633.
[4]. Lewandowski, A.; Swiderska-Mocek, A. *J. Power Sources* **2009**, *194(2)*, 601-609.
[5]. DuPasquier, A.; Warren, P. C.; Culver, D.; Gozdz, A. S.; Amatucci, G. G.; Tarascon, J. M. *Solid State Ionics* **2011**, *135*, 249-257.
[6]. Fergus, J. W. *J. Power Sources* **2010**, *195(15)*, 4554-4569.
[7]. Bonne, M.; Pronier, S.; Can, F.; Courtois, X.; Valange, S.; Tatibouet, J. M.; Royer, S.; Marecot, P.; Duprez, D. *Solid State Sci.* **2010**, *12(6)*, 1002-1012.

[8]. Cao, J.; Wang, L.; Shang, Y.; Fang, M.; Deng, L.; Gao, J.; Li, J.; Chen, H.; He, X. *Electrochim. Acta* **2013**, *111*, 674-679.
[9]. Kurc, B. *Electrochim. Acta* **2014**, *125*, 415-420.
[10]. Murthy, S. N. *The Rigaku Journal* **2004**, *21*, 15-24.
[11]. Sakka, S. Handbook of sol-gel science and technology processing characterization and applications. Kozuka S. Kluwer Academic Publishers, 2005.
[12]. Martyla, A.; Olejnik, B.; Kirszensztejn, P.; Przekop, R. *Int. J. Hydrogen Energ.* **2011**, *36*, 8358-8364.
[13]. Kirszensztejn, P.; Kawałko, A.; Tolinska, A.; Przekop, R. *J. Porous Mater.* 2011, *18*, 241-249.
[14]. Tomer, V.; Manias, E.; Randall, C. A. *J. Appl. Phys.* **2011**, *110*, 044107.
[15]. Thanganathan, U.; Nogami, M. *RSC Advances* **2012**, *2*, 9596-9605.
[16]. Stephan, A. M.; Nahm, K. S.; Kumar, T. P.; Kulandainathan, M. A.; Ravi, G.; Wilson, J. *J. Power Sources* **2005**, *159 (2)*, 1316-1321.
[17]. Wieczorek, W.; Steven, J. R.; Florjanczyk, Z. *Solid State Ionics* **1996**, *85*, 67-72.
[18]. Ulaganathan, M.; Nithya, R.; Rajendran, S.; Raghu, S. *Solid State Ionics* **2012**, *218*, 7-12.
[19]. Ataollahi, N.; Ahmad, A.; Hamzah, H.; Rahman, M. Y. A.; Mohamed, N. S. *J. Electro. Sci.* **2012**, *7*, 6693-6703.
[20]. Balachandran, K.; Venckatesh, R.; Sivaraj, R. *Int. J. Eng. Sci. Tech.* **2010**, *2(8)*, 3695-3700.
[21]. Saikia, D.; Chen-Yang, Y. W.; Chen, Y. T.; Li, Y. K; Lin, S. I. *Desalination* **2008**, *234*, 24-32.
[22]. Zhang, H. Z.; Banfield, J. F. *J. Mater. Res.* **2000**, *15, 437-448.*
[23]. Li, Y.; Sun, X.; Li, H.; Wang, S.; Wei, Y. *Powder Tech.* **2009**, *194*, 149-152.
[24]. Osinska, M.; Zalewska, A.; Jesionowski, T.; Walkowiak, M. *J. Membrane Sci.* **2009**, *326*, 582-588**.**
[25]. Walkowiak, M.; Osinska, M.; Jesionowski, T.; Siwinska-Stefanska, K. *Cent. Eur. J. Chem.* **2010**, *8(6)*, 1311-1317.
[26]. Miao, R.; Liu, B.; Zhu, Z.; Liu, Y.; Li, J.; Wang, X.; Li, Q. *J. Power Sources* **2008**, *84(2)*, 420-426.
[27]. Caillon-Caravanier, M.; Claude-Montigny, B.; Lemordant, D.; Bosser, G. *J. Power Sources* **2002**, *107*, 125-132.
[28]. Wu, C. G.; Lu, M. I.; Tsai, C. C.; Chuang, H. J. *J. Power Sources* **2006**, *159(1)*, 295-300.
[29]. Jeon, J. D.; Kim, M. J.; Chung, J. W.; Kwak, S. I. NSTI Nanotech 2005, ISBN 0-9767985-1-4, 2005, 2.
[30]. Li, G.; Li, Z.; Zhang, P.; Zhang, H.; Wu, Y. *Pure Appl. Chem.* **2008**, *80*, 2553-2563.